

CrossMark
click for updatesCite this: *J. Mater. Chem. A*, 2015, 3,
314

Addressing the light-soaking issue in inverted organic solar cells using chemical bath deposited fluorinated TiO_x electron transport layer†

Fang Jeng Lim,^{ab} Ying Ting Set,^b Ananthanarayanan Krishnamoorthy,^b
Jianyong Ouyang,^{bc} Joachim Luther^d and Ghim Wei Ho^{*a}

The device lifetime of an inverted organic solar cell (IOSC) is significantly better compared to standard-architecture OSC under ambient conditions. However, various studies have shown that when an n-type oxide is used as a selective electron transport layer (ETL) in the IOSC, a reversible light-soaking treatment is required. This reversible treatment largely hampers the practicality of the device, especially in outdoor applications, in which the light-soaking time may take hours every morning. In this work, fluorinated TiO_x (F-TiO_x), prepared by low-temperature solution-processed chemical bath deposition technique, was used as the ETL to significantly reduce the light-soaking time for a P3HT:PCBM based IOSC. Without affecting the device efficiency, more than ten-fold reduction in light-soaking time was observed for fluorinated TiO_x (F-TiO_x) when compared with conventional sol-gel TiO_x. Ultraviolet photoelectron spectroscopy (UPS) and UV photoconductivity measurements were used to understand the light-soaking time reducing mechanism. From the perspective of ITO/TiO_x interface, shift in work function was observed in F-TiO_x due to the partial filling of its defective sites by fluorine atoms. Consequently, this process reduces its intrinsic trap state density compared to sol-gel TiO_x even before the light-soaking treatment. As a result, the trap filling action can be completed in a shorter time upon illumination, and thus significantly reduce the duration of the necessary light-soaking.

Received 24th September 2014
Accepted 23rd October 2014

DOI: 10.1039/c4ta05042h

www.rsc.org/MaterialsA

1 Introduction

Impressive progress in the forms of superior air-stability and increasing device efficiency in the development of inverted organic solar cells (IOSCs) has recently been reported.^{1–4} However, there is an inherent issue, *i.e.*, the necessity of a mandatory “light-soaking” treatment, in which the device needs to be exposed to light with UV components to improve the device characteristics.⁵ This phenomenon is commonly observed in IOSCs with n-type oxide semiconductors (TiO_x, ZnO) as a selective electron transport layer (ETL). The as-prepared device initially shows s-shaped current density–voltage characteristics, a low short circuit current and low fill factor.^{5–8} After prolonged illumination (~10 min under AM 1.5G

irradiation), the device efficiency gradually improves and saturates at the highest value. The light-soaking behavior in the IOSC appears to originate from the necessary filling of the defective trap sites in the oxide semiconductor layer by the photoelectrons generated by the UV component ($\lambda \leq 400$ nm) in the AM 1.5G illumination (1000 W m^{-2}).^{5,9} Such trap filling action would consequently lower the work function of the ETL and improve its electron selectivity.^{5,10} It is important to note that the light-soaking effect is reversible.^{11–13} As a result, the device would have to be light soaked repeatedly at each light–dark cycle (every morning if used for outdoor applications), and this requirement largely hinders the device practicality. In laboratory testing (AM 1.5G, 1000 W m^{-2}), typical IOSC devices require at least 10 min to complete the light-soaking;^{3,5,14} in outdoor applications, the same device would require at least an hour of light-soaking every morning. Therefore, it would be highly beneficial to significantly reduce the light-soaking time in inverted organic solar cells. Strontium- and barium-doped ZnO and Al-doped ZnO on TiO_x (AZO–TiO_x) have already been used as the ETL in attempts to address this issue with the IOSC.^{7,10}

We hereby report on the use of fluorinated TiO_x (F-TiO_x), deposited by chemical bath deposition (CBD), as a functionalized electron transport layer in the IOSC to address the light-soaking issue. This material has been applied extensively in

^aDepartment of Electrical and Computer Engineering, National University of Singapore, Blk EA #06-10, 9 Engineering Drive 1, 117575 Singapore, Singapore. E-mail: elehw@nus.edu.sg; Fax: +65 6775 4710; Tel: +65 6516 8121

^bSolar Energy Research Institute of Singapore (SERIS), National University of Singapore, 7 Engineering Drive 1, 117574 Singapore, Singapore

^cDepartment of Material Science and Engineering, National University of Singapore, Blk E4 #01-01, 9 Engineering Drive 1, 119260 Singapore, Singapore

^dFraunhofer Institute for Solar Energy Systems, Heidenhofstr. 2, 79110 Freiburg, Germany

† Electronic supplementary information (ESI) available. See DOI: 10.1039/c4ta05042h

various applications, such as electrochromic applications,¹⁵ the anti-corrosion of metal,¹⁶ photocatalytic applications¹⁷ and solar cells.¹⁸ The presence of fluorine in TiO_x could significantly reduce its dangling bonds by passivation.¹⁵ In CdS and CdSe quantum dot solar cells (QDSC), F-TiO_x was used to enhance cell efficiency.¹⁸ Chemical bath deposition (CBD) is a routinely employed coating technique to fabricate metal oxide thin films.^{19,20} It is a facile, scalable, low temperature, solution processed and low-cost deposition method. Oxide thin films can be deposited by immersing a substrate in a chemical bath of the precursor solutions.²¹ Furthermore, a straightforward thickness control in the range of 20 nm to several microns can be achieved.^{22–25} This technique is normally adopted for the fabrication of transparent conducting oxide (TCO)²⁰ and active layer in thin film transistors.²⁶ In solar cell applications, CBD has been used to fabricate well-controlled TiO_x layers.^{22,27} This technique can also be utilised to deposit a uniform TiO_x layer on larger TCO substrates with relative ease compared with the conventional spin coating technique. The incorporation of fluorine into TiO_x can also be intrinsically performed by CBD onto TCO substrates.^{15,16} To the best of our knowledge, this material has not been previously used in OSC applications, and there has been no report on addressing the light-soaking issue in IOSC devices using a chemical bath deposited ETL.

In this work, we demonstrate the use of the as-deposited (CBD) fluorinated TiO_x (F-TiO_x) as the electron transport layer in a P3HT:PCBM based inverted organic solar cell. Without affecting the device efficiency, its light-soaking time was reduced by more than ten-fold compared to IOSCs with conventional sol-gel coated TiO_x as electron transport layer. A model from the perspective of the ITO/TiO_x interface was suggested to explain the possible cause of reduction in light-soaking time.

2 Results and discussions

The inverted organic solar cells with F-TiO_x interlayer were fabricated as described in detail in the Experimental section. The device architecture was ITO/F-TiO_x/P3HT:PCBM/PEDOT:PSS-CFS31/Ag, as shown in Fig. 1. The corresponding cross section SEM image of the device is attached to the schematics in the same figure. An IOSC device with architecture ITO/

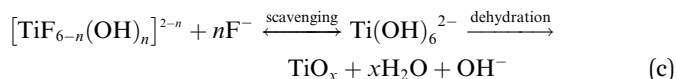
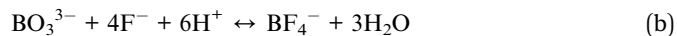
sol-gel TiO_x/P3HT:PCBM/PEDOT:PSS-CFS31/Ag, which was reported earlier,³ was used as a control device in this work.

Metal oxide electron transport layer characterization

The deposition reaction in CBD consists of hydrolysis equilibrium reaction of a metal-fluoro complex ((NH₄)₂TiF₆) and the consumption reaction of F⁻ from its ion scavenger (H₃BO₃). For the hydrolysis reaction, Deki *et al.* proposed the following reaction scheme:²⁸



The addition of H₃BO₃ readily reacts with the F⁻ ion produced in reaction (a) to form the more stable complex ion BF₄⁻, as shown in reaction (b). According to the law of mass action, the equilibrium of reaction (a) will shift to the right due to the consumption of fluoride ions. According to their studies, Deki *et al.* have shown that apart from reacting with free fluoride ions, BO₃³⁻ also reacts with the ions in the [TiF_{6-n}(OH)_n]²⁻ⁿ. This reaction triggers the formation of [Ti(OH)₆]²⁻, which forms TiO_x after dehydration (reaction (c)).²⁸ The nucleation of TiO_x occurs in the chemical bath, causing the solution to become cloudy. Because of the environment of the chemical bath, fluorine ions readily adsorb onto the TiO_x layers, thus forming fluorinated TiO_x (F-TiO_x).



Because the deposition of F-TiO_x as electron transport layer for organic solar cell applications was not previously reported, the optimal precursor concentration and the optimal F-TiO_x thickness for maximum efficiency (η) were determined in this investigation. We determined that, in various concentrations of (NH₄)₂TiF₆, the deposition rate can be varied from 35 nm h⁻¹ to 65 nm h⁻¹ (see ESI† for details). This variation in deposition rate was determined to affect the resulting F-TiO_x film morphology.

The film morphology of the ETL is critical, as it determines whether a proper selective contact can be established with the adjacent photoactive layer. It was determined that at different (NH₄)₂TiF₆ concentration regimes, islands, cracks or smooth TiO_x film were observed. At a low concentration (0.02 M and 0.03 M, Fig. 2(a) and (b)) of (NH₄)₂TiF₆, F-TiO_x islands were formed and these islands could cause an increase in series resistance because of improper contact between the ETL with the photoactive layer. Thus, the presence of islands is detrimental for device performance. Cracks were formed in the F-TiO_x when the deposition rate was relatively high (0.05 M (NH₄)₂TiF₆), as clearly observed in Fig. 2(c). When the formation of TiO_x accelerates, stress is introduced on the film and eventually forms cracks on the surface. These cracks form the recombination centers and deteriorate the electronic coupling at the TiO_x/organic interface, increasing the loss due to

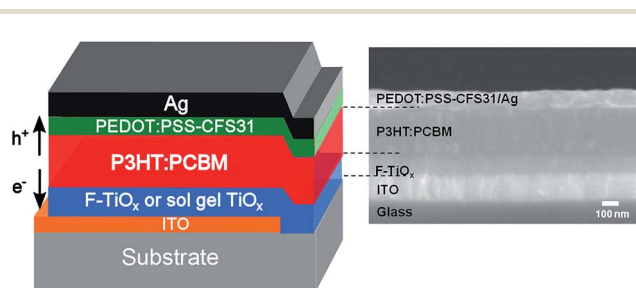


Fig. 1 Illustration of the device architecture for inverted organic solar cells investigated in this study (left) and the corresponding cross section SEM image (right).

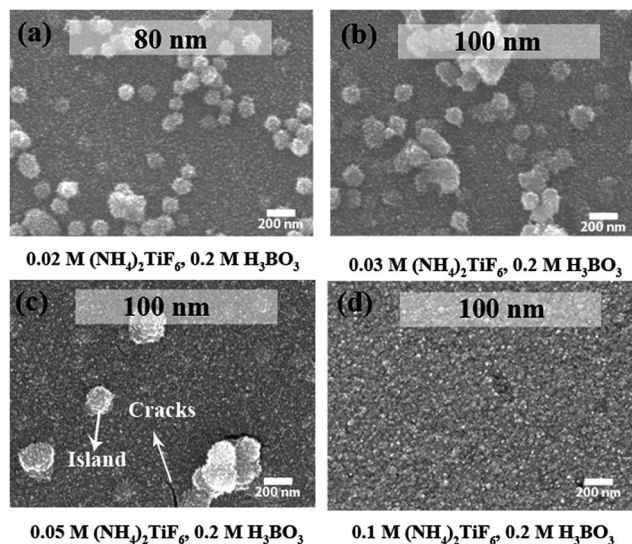


Fig. 2 SEM topographic images showing film morphology of F-TiO_x on ITO. The samples were prepared with (a) 0.02 M, (b) 0.03 M, (c) 0.05 M, and (d) 0.1 M (NH₄)₂TiF₆ at fixed 0.2 M H₃BO₃. The thickness of the reported F-TiO_x layers are 100 nm, except for (a), for which the film growth stops at 80 nm.

recombination.²⁹ Therefore, the presence of cracks is not beneficial for IOSCs. In the region of 0.1 M (NH₄)₂TiF₆ and 0.2 M H₃BO₃, the morphology of the film is least defective, without the presence of islands and cracks at a thickness of 100 nm (Fig. 2(d)). The deposited F-TiO_x film also has decent coverage over the ITO substrate. Such coverage would help in minimizing the likelihood of highly resistant and improper contact with the photoactive layer. Hence, by correlating the deposition rate and the F-TiO_x film morphology, the precursor concentrations were set at 0.1 M (NH₄)₂TiF₆ and 0.2 M H₃BO₃.

Fig. 3(a) and (b) show the summary of the thickness of the resulting F-TiO_x film at various (NH₄)₂TiF₆ concentration with 0.2 M H₃BO₃ and the deposition rate as a function of the two precursor concentrations. The red contour lines in Fig. 3(a) and (b) indicate the speculated optimal region for a relatively efficient IOSC. For validation, IOSC devices with F-TiO_x deposited at various precursor concentrations were fabricated. The efficiency (η) and the fill factor of the devices under AM 1.5G illumination are shown in Fig. 3(c). The film grown with 0.05 M (NH₄)₂TiF₆ expectedly gives a lower η (2.5%), because of a low fill factor (54%), indicating an improper contact between the ETL and the P3HT:PCBM layer because of the presence of islands and cracks. As the precursor concentration increases, the fill factor gradually increases and remains constant at 60%. The F-TiO_x deposited at 0.1 M (NH₄)₂TiF₆ gives the highest efficiency (3%), with a high fill factor (60%). At this concentration, the optimal F-TiO_x thickness was determined to be 80 nm, which gives the highest η of 3% (Fig. 3(d)). Hence, the F-TiO_x film with a thickness of 80 nm, deposited with 0.1 M (NH₄)₂TiF₆ and 0.2 M H₃BO₃ was adopted for further studies in this work.

It has been experimentally demonstrated that NaOH is able to remove fluorine atoms adsorbed onto a TiO_x surface by

replacing them with hydroxyl groups.³⁰ This treatment can also convert the physically adsorbed F into Ti-bonded F.¹⁷ Wang *et al.* reported that if fluorinated TiO_x is washed with NaOH and water, the concentration of Ti-bonded F can be increased.³¹ Thus, this method was also used in the present study to alter the fluorine content in the samples. X-ray photoelectron spectroscopy (XPS) was used to determine the fluorine atomic concentration on the TiO_x surface. Fig. 4(a) shows the F 1s spectra for the sol-gel TiO_x and F-TiO_x subjected to various post treatments. It was determined that, in addition to the sol-gel TiO_x, a peak at 688.6 eV was observed for all F-TiO_x samples. This peak is attributed to Ti-bonded F in TiO_x and not the adsorbed fluorine, for which a peak around 684.4 eV is generally observed.³² Elemental analysis shows that the as-prepared F-TiO_x contains 1.3 at% of fluorine. As shown in Fig. 4(b), the amount of fluorine increases to 1.5 at% and 1.7 at% after the samples were subjected to NaOH and water post treatments, respectively. To validate the results, analysis of the Ti 2p and O 1s spectra (not shown in the figure) for the samples, to obtain the ratio of atomic concentrations between Ti-O and OH (hydroxyl) bonds, was carried out. The Ti-O : OH ratio of various samples in Fig. 4(b) shows that after the post treatments, the concentration of the OH group increases. This result correlates well with the increase in Ti-bonded F concentration, suggesting that the post treatments remove the surface F and replace them by OH groups, which is in line with earlier reports.³¹ Then, the removed fluorine can fill in the incomplete Ti-O-Ti matrix, which leads to increase in fluorine concentration in F-TiO_x. For detailed studies in the next section, a device with sol-gel TiO_x (0 at% fluorine) as ETL is used as the control.

Device performance

Table 1 shows the solar cell characteristics of devices with TiO_x ETL at various fluorine atomic concentrations. While the open circuit voltages (V_{oc}) of all the devices were similar, the short circuit current density (j_{sc}) of the sol-gel TiO_x, as-prepared F-TiO_x and NaOH treated F-TiO_x are similar (7.5 mA cm⁻²), while the H₂O treated F-TiO_x sample gives a slightly higher j_{sc} (8 mA cm⁻²). However, this effect was traded off with a decrease in fill factor (62%) compared to the as-prepared F-TiO_x. As a result, the cell efficiencies were not altered by the presence of fluorine in TiO_x (3.0%).

However, the devices exhibited a significant difference when they were subjected to light-soaking, as shown in Fig. 5. Fig. 5(a) and (b) show the j - V characteristics for sol-gel TiO_x and the as-prepared F-TiO_x based IOSC devices, respectively, under AM 1.5G conditions (light-soaking treatments). S-shape characteristics were observed at the initial stage of illumination. The s-shape is a typical effect, which occurs due to the suppression in electron transport in TiO_x, which results in a high resistance.³³ It is noteworthy that the F-TiO_x device reaches its maximum efficiency (50 s), considerably faster compared to the sol-gel TiO_x device (350 s), after light-soaking. Fig. 5(c) shows the time evolution of device efficiency with various F atomic concentrations under AM 1.5G illumination in N₂ atmosphere. The experimental data was fitted with a logistic function (see eqn

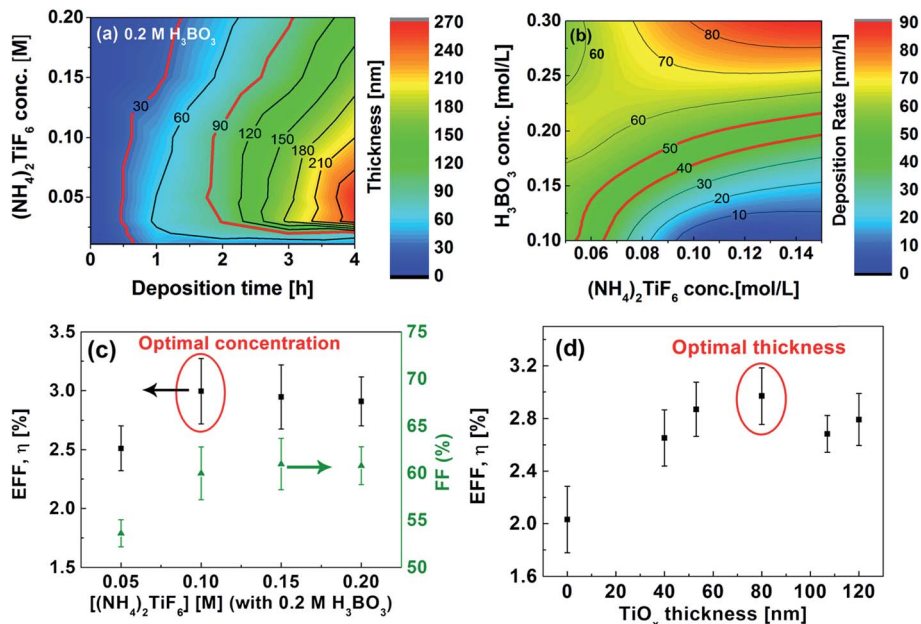


Fig. 3 Color contour representation of (a) F-TiO_x thickness over time at various (NH₄)₂TiF₆ concentrations (fixed 0.2 M H₃BO₃). (b) Deposition rate of F-TiO_x at various precursor concentrations. The red contour lines indicate the regions of desired thickness and film morphology for the F-TiO_x ETL. (c) Efficiency (■) and fill factor (▲) of inverted organic solar cells with F-TiO_x ETL deposited using various concentrations of (NH₄)₂TiF₆ and 0.2 M H₃BO₃. (d) Efficiency at various F-TiO_x thicknesses in inverted OSC device. All the data points were averaged for at least 5 reproducible devices. The respective error bars represent the standard deviation of each type of device.

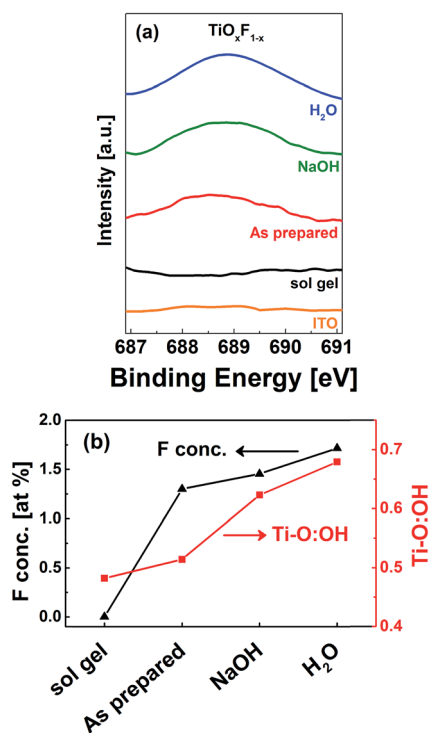


Fig. 4 (a) F 1s photoelectron spectra for various TiO_x samples on ITO substrate. The F 1s XPS spectra indicates the presence of adsorbed fluorine (~688.6 eV) in all CBD F-TiO_x devices. (b) Elemental analysis showing the atomic concentration of F and Ti-O:OH ratio on the sample surfaces corresponds to sol gel TiO_x and the as-prepared, NaOH treated and H₂O treated F-TiO_x.

(S1) and Table S2† for fitting function and parameters). By defining the light-soaking time (τ_{soak}) as the time required for the efficiency to reach 95% of its maximum value ($\eta(\tau_{\text{soak}}) = 0.95\eta_{\text{max}}$), the light-soaking effect for various devices was quantified, and are shown in Table 1. Devices with 0 at% fluorination (sol-gel TiO_x) require approximately 450 seconds for the η to saturate, close to the values in previous reports.^{6,12} It is noteworthy that 450 s (8 min) of light soaking time in indoor laboratory conditions would require at least 1 h of light-soaking at outdoor conditions every morning (see Fig. S1† for rough calculations). For the as-prepared CBD F-TiO_x devices (1.3 F at%), the η saturates in approximately 35 s of illumination. However, for NaOH treated F-TiO_x (1.5 F at%), τ_{soak} increases to approximately 520 s and H₂O treated F-TiO_x (1.7 F at%) shows 110 s for τ_{soak} . All the post treated CBD F-TiO_x samples, although having higher amounts of fluorine concentration, did not have shorter soaking time compared with 0 F at% TiO_x. This result may suggest that OH groups on the TiO_x surface could be the cause of trap formation, which leads to the necessity of light-soaking treatment. Nevertheless, the as-prepared F-TiO_x, without further post treatments, can be used to address the light-soaking effect in inverted organic solar cells to significantly reduce the light-soaking time by a factor of 13 (450 s to 35 s) compared to devices with sol-gel TiO_x ETL. As a result, a comparison of the as-prepared F-TiO_x with sol-gel TiO_x was performed in order to further understand the underlying reason for this light-soaking enhancement.

The device stability of the as-prepared IOSC with F-TiO_x ETL was investigated by storing the sample in dark, at ambient conditions and monitoring its efficiency (η) over time, in

Table 1 Photovoltaic parameters of IOSCs at various fluorine concentration in TiO_x (j_{sc} : short circuit current density, V_{oc} : open circuit voltage, FF: fill factor, η : efficiency, τ_{soak} : light-soaking time). The active area of all the devices was 0.09 cm^2 . The error values correspond to the standard deviation of the device parameters of at least 10 reproducible cells

Process	F at%	V_{oc} [$\pm 17 \text{ mV}$]	j_{sc} [$\pm 0.3 \text{ mA cm}^{-2}$]	FF [$\pm 4\%$]	η [$\pm 0.3\%$]	τ_{soak} [s]
Sol-gel	0	628	7.5	62	2.9	450
CBD (as-prepared)	1.3	617	7.6	63	3.0	35
CBD (NaOH treated)	1.5	623	7.5	62	2.9	520
CBD (H_2O treated)	1.7	615	8.0	62	3.0	110

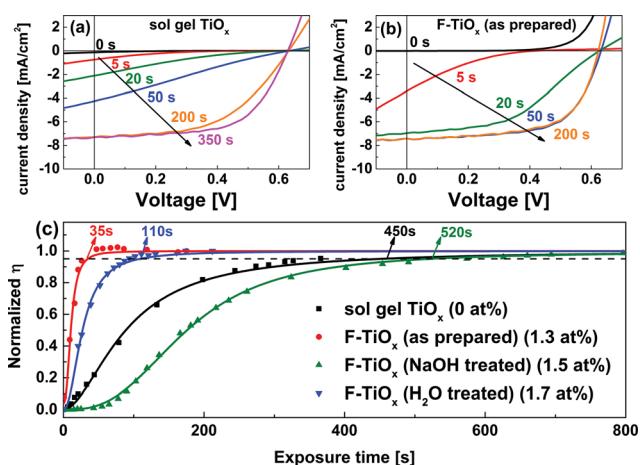


Fig. 5 Current density–voltage (j – V) characteristics of inverted organic solar cells with (a) sol-gel TiO_x and (b) as prepared F-TiO_x (1.3 F at%) as electron transport layer when subjected to light-soaking treatments, in which the illumination times are shown (guided by arrows). (c) Light-soaking effect on the efficiency of fresh devices with TiO_x layers upon AM 1.5G illumination. The symbols represent experimental data, while the solid lines are fitted data by logistic function. The indicated time represents the corresponding light-soaking time (τ_{soak}) for each sample, as defined in the main text.

accordance with the International Summit on Organic Photovoltaic Stability (ISOS) D-1 shelf scheme.³⁴ Fig. 6 shows the normalized open circuit voltage (V_{oc}), short circuit current density (j_{sc}), fill factor and η of the as-prepared CBD F-TiO_x over a period of 1000 h, stored in a dark environment without encapsulation. The device shows superior stability over the non-encapsulated standard architecture OSC (inset), which was determined to be fully degraded in less than 24 h. The as-prepared F-TiO_x device was able to retain 60% of its initial device performance even after 1000 h. The main cause of degradation is associated with the short circuit current density, as shown in Fig. 6 (red line). During the 70 h in presence of air, the device efficiency slightly increases compared to the freshly prepared cells. This initial increase was because of the increase in V_{oc} . This phenomenon can be attributed to the oxidation of silver to silver oxide when stored at ambient condition. The work function is increased, which in turn increases the V_{oc} .^{35,36} j_{sc} decrease may be due to the ingress of oxygen from the silver contact and moisture from the PEDOT:PSS to the photoactive layer, which may cause both chemical and physical changes in the photoactive layer.³⁴ Overall, this result reveals that the

incorporation of fluorine into TiO_x has no detrimental effect on the photoactive layer, P3HT:PCBM, and the IOSC device performance.

Physical studies on the light-soaking characteristics

Several reports have suggested that the light-soaking behavior of an IOSC device with metal oxide ETL originates from at least two perspectives. Firstly, the light-soaking originates from the filling of trap states, which decreases the work function of the ETL and enables the electron extraction through the ITO/metal oxide interface.⁵ Secondly, the induced interfacial dipole between the metal oxide/organic interface may also determine the formation of an extraction barrier for the dissociated excitons in the device.¹⁰ In view of the new material (F-TiO_x) proposed in this work, we could not rule out the effects by any one of them. Thus, we have conducted a control light-soaking experiment with various ETLs, such as sol-gel TiO_x (80 nm), F-TiO_x (80 nm), bilayer sol-gel TiO_x (40 nm)/ F-TiO_x (40 nm) and F-TiO_x (40 nm)/sol-gel TiO_x (40 nm), to investigate which interface contributes to the light-soaking behavior (see Experimental section for film preparation). The results in Fig. 7 show that the F-TiO_x based device has the shortest light-soaking time (~ 30 s), followed by the sol-gel TiO_x / F-TiO_x (~ 150 s), F-TiO_x /sol-gel TiO_x (~ 170 s) and sol-gel TiO_x (~ 450 s). This observation suggests that both ITO/ TiO_x and TiO_x /organic interfaces

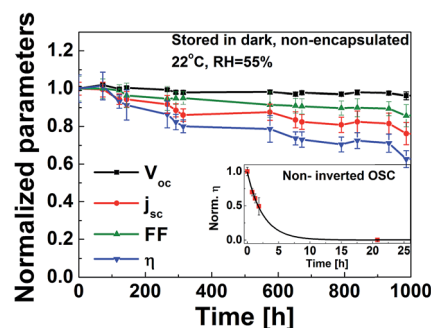


Fig. 6 Normalized V_{oc} , j_{sc} , fill factor, η of ITO/CBD F-TiO_x /P3HT:PCBM/PEDOT:PSS/Ag (without encapsulation) over 1000 h subjected to ISOS-D-1 scheme (stored in dark shelf, open circuit condition at 22°C , R.H. 55%). The inset shows the degradation of the non-encapsulated standard architecture OSC (ITO/PEDOT:PSS/P3HT:PCBM/LiF/Al) under the same conditions. The error bar corresponds to the standard deviation of each parameter for 10 reproducible devices.

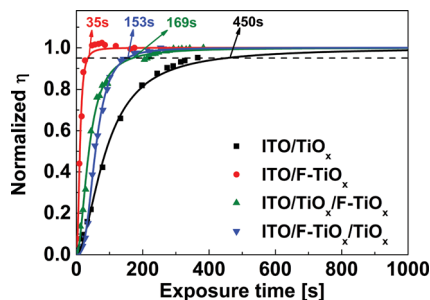


Fig. 7 Light-soaking control experiment of fresh inverted organic solar cells with sol-gel TiO_x (80 nm), F- TiO_x (80 nm), sol-gel TiO_x (40 nm)/F- TiO_x (40 nm) and F- TiO_x (40 nm)/sol-gel TiO_x (40 nm) as electron transport layers upon AM 1.5G illumination. The symbols represent experimental data, while the solid lines are fitted data by logistic function. The indicated time represents the corresponding light-soaking time (τ_{soak}) for each sample, as defined in the main text.

contribute to the light-soaking behavior, as seen from the intermediate timings compared to that of pure sol-gel TiO_x . In this work, we first examined the effect of trap-filling at the ITO/ TiO_x interface on the light-soaking behavior.

The necessity of light-soaking seems to originate from the active unfilled electron traps caused by dangling bonds.^{5,7,10} These dangling bonds are susceptible to the adsorption of oxygen from air to form active trap sites, which could then be removed by UV photons.⁹ The presence of active traps affects the position of the quasi Fermi level for the electrons and the trap state density in the material. These two dominant parameters can be measured *via* ultraviolet photoelectron spectroscopy (UPS) and transient UV photoconductivity measurements, respectively. Through these techniques, the role of fluorine atoms on the light-soaking behavior of these amorphous TiO_x thin films (see Fig. S3† for XRD spectra) was studied.

UPS technique was used to investigate the effect of fluorine atoms in TiO_x on the light-soaking time from the energetics perspective. It was carried out by measuring the vacuum level shifts of sol-gel TiO_x and F- TiO_x films with respect to that of the ITO before light-soaking. Fig. 8(a) shows the region near the secondary electron cutoff and the emission onset for ITO, ITO/sol-gel TiO_x (0 F at%) and ITO/F- TiO_x (1.3–1.7 F at%) before light-soaking. A vacuum level shift (ΔE_{vac}) of 0.41 eV between the ITO and sol-gel TiO_x interface was observed. In the presence of fluorine, a total ΔE_{vac} of 0.51 eV (0.41 + 0.10 eV) was observed. Therefore, F- TiO_x has a lower work function (4.4 eV) than sol-gel TiO_x (4.5 eV), as summarized in Fig. 8(b). Because all the films were subjected to the same heat treatment (180 °C), we can associate the change in work function to be largely dependent on the presence of fluorine incorporation into TiO_x . These UPS measurements suggest a shift of Fermi level at the ITO/ TiO_x interface.

TiO_x is known to exhibit transient UV photoconductivity with long charging and relaxation times, due to the large amount of surface trap states.^{5,37} These trap states cause a decrease in the overall mobile carrier concentration of the material, and thus its conductivity. Transient UV photoconductivity measurements of sol-gel TiO_x and F- TiO_x (1.3 at%), before and after UV

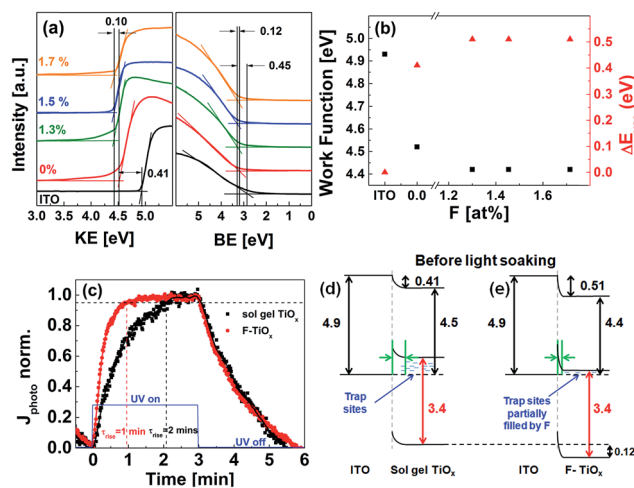


Fig. 8 (a) Ultraviolet photoelectron spectroscopy (UPS) secondary cut-off spectra of ITO and ITO/ TiO_x samples of various fluorine concentrations before light-soaking. The binding energy (BE) was set to zero at the Fermi level. (b) Work function values (■) and vacuum level shift (ΔE_{vac} , ▲) at ITO/ TiO_x interface. (c) Normalized photocurrent of sol-gel TiO_x (0 at%)/Ag (■) and F- TiO_x (1.3 F at%)/Ag (●) under UV illumination. The blue line (—) indicates UV light ON/OFF state. (d and e) Resulting energy band diagrams at ITO/ TiO_x interface before light-soaking treatment. All values were obtained from UPS measurements, the band gaps were estimated by their respective absorption spectra (see Fig. S4†), and the green arrows at the ITO/ TiO_x interface represent the resulting barrier width due to Fermi level realignment.

illumination, were carried out to investigate the existence of the traps and the filling characteristics of the traps. Fig. 8(c) shows the normalized photocurrent of sol-gel TiO_x /Ag and the as-prepared CBD F- TiO_x /Ag devices under UV illumination. At initial illumination, the trap states were gradually filled by photogenerated electrons in TiO_x , increasing the overall mobile charge carrier concentration, and hence the photocurrent. For a detailed analysis, we define photocurrent rise time (τ_{rise}) as the time required for the photocurrent to reach 95% of its maximum value, indicating the time required for a complete trap filling. It is noteworthy that τ_{rise} of F- TiO_x (1.3 at%) (1 minute) is twice as fast compared with that of sol-gel TiO_x (2 min). Because the saturation of the photocurrent at constant illumination implies equilibrium between the trapping action and charge recombination,⁵ a shorter τ_{rise} would suggest that the material has a lower amount of trap states. Hence, we may conclude that the trap state density in the F- TiO_x (1.3 at%) layer is considerably lower than that in sol-gel TiO_x .

By combining the findings of the UPS spectra and the UV photoconductivity response, we suggest an explanation for the improvement in the light-soaking characteristics of the device with fluorinated TiO_x electron transport layer from the perspective of the ITO/ TiO_x interface. Fig. 8(d) and (e) show the resulting energy level diagrams of the interfaces for sol-gel TiO_x and F- TiO_x before light-soaking. In sol-gel TiO_x , due to the lower ΔE_{vac} (0.41 eV) and higher work function (4.5 eV), the Fermi level (E_{F}) is farther away from the conduction band. Because there are more trap states in sol-gel TiO_x , the shift of E_{F} suggests that the material has a lower overall carrier

concentration due to these unfilled trap states. This phenomenon would influence its barrier width at the ITO/TiO_x interface, which is related to Debye length (L_D), a characteristic length scale for charge screening.¹⁰ L_D scales with the dielectric constant (ϵ) and the carrier concentration (n) ($L_D \propto (\epsilon/n)^{0.5}$). A lower carrier concentration would result in a large L_D , and thus forms a larger barrier width (green arrow) between ITO and sol-gel TiO_x (Fig. 8(d)).

In F-TiO_x, due to the higher ΔE_{vac} (0.51 eV) and the lower work function (4.4 eV), with an observable shift of 0.12 eV of the valence band to higher binding energy (Fig. 8(a)), E_F shifts closer to the conduction band compared with that of sol-gel TiO_x. Because the trap state density of F-TiO_x is lower compared to sol-gel TiO_x, the shift in E_F suggests an increase in overall carrier concentration, probably due to partial filling of the electron trap sites by fluorine atoms in the TiO_x. The increased carrier concentration decreases the L_D and narrows the barrier width (green arrow) between ITO and F-TiO_x (Fig. 8(e)). This result also corroborates with a recent study that shows a significant increase in a carrier concentration of TiO₂ after doping with fluorine.³⁸ It is noteworthy that all these phenomena are observed at the ITO/TiO_x interface before light-soaking treatment.

When the device is illuminated, the ΔE_{vac} of both TiO_x and F-TiO_x samples increases, and it is highly possible that they will have similar values because of their identical cell efficiencies (3.0%). As a result, their ΔE_{vac} values would converge towards about 0.6 eV after light-soaking, as observed by Kim *et al.*⁵ Given that the initial ΔE_{vac} value of F-TiO_x (0.5 eV) is nearer to that of the light-soaked condition (0.6 eV), the time taken to fully fill the trap sites in F-TiO_x is significantly shorter compared to sol-gel TiO_x, as observed in Fig. 5(c). Hence, these findings provide a possible explanation for the significant reduction in the light-soaking time in F-TiO_x inverted organic solar cells.

Given the same reduced work function, the NaOH (1.5 at%) and H₂O (1.7 at%) treated F-TiO_x samples show inferior light-soaking effect. This phenomenon leads to the idea that the ITO/TiO_x interface may not be the only factor in influencing the light-soaking effect. The modification of the TiO_x surface by these treatments suggests that there is an induced dipole at the TiO_x/organic interface, which may also play a certain role in the light-soaking effect. An extended study from this perspective will be performed in future.

3 Conclusion

The application of fluorinated TiO_x (F-TiO_x) as the electron transport layer (ETL) was used to address the light-soaking issue in inverted organic solar cells (IOSC). The ETL was fabricated by a solution processed chemical bath deposition method. The presence of fluorine in TiO_x seems to reduce the trap state density in the ETL by partially filling the states and causing a decrease in its work function before light-soaking is carried out. The effect significantly shortens the time required for trap filling when the device is illuminated. Therefore, the use of F-TiO_x, without further post treatments, can significantly decrease the necessary light-soaking time by a factor of 13 (from

450 s to 35 s) in an air-stable inverted organic solar cell (IOSC) compared with the time for its sol-gel TiO_x counterpart without affecting device efficiency. This material can significantly increase the practicality of an air-stable, efficient and solution-processed inverted organic solar cell.

4 Experimental

Materials

Titanium isopropoxide (TTIP, 97%, Sigma-Aldrich), acetylacetone (AA, Sigma-Aldrich) and isopropanol (IPA, reagent grade, Aik Moh Paints & Chemical Pte Ltd.) were used to prepare the sol-gel TiO_x electron transport layer. For the chemical bath deposited F-TiO_x, ammonium hexafluorotitanate ((NH₄)₂TiF₆, 99.99%, Sigma-Aldrich) and boric acid (H₃BO₃, ≥99.99%, Sigma-Aldrich) were used. Regioregular (>98%) poly(3-hexylthiophene) (P3HT, product code M101, average M_w 65 500, Ossila), phenyl-C₆₁-butyric acid methyl ester (PC₆₁BM – 99.5% purity, product code Nano-CPCBM-BF, Nano-C) and poly(3,4-ethylenedioxythiophene):poly(styrene sulfonate) (PEDOT:PSS – Heraeus Clevis P VP AI 4083, product code M121, Ossila) were used as donor, acceptor and hole transport layer, respectively. 1,2-Dichlorobenzene (DCB, Sigma-Aldrich) was used as the solvent for donor and acceptor. Capstone® FS-31 (Dupont) was added into PEDOT:PSS prior to spin coating. Silver (Ag) metal was purchased from K. J. Kurt Lesker & Co. All the above-mentioned materials were used as received.

Solution preparation

The sol-gel TiO_x precursor solution was prepared by adding an appropriate amount of acetylacetone dropwise to TTIP under continuous stirring. Then, isopropanol was added to the mixture as solvent. The volume ratio of TTIP : AA : IPA was set to 1 : 0.5 : 10. Then, the solution was stirred for at least 2 h prior to spin coating onto the substrate. The as-prepared solution exhibits an orange-yellow color, indicating the d-d absorption originating from the titanium complex ion formed by the reaction between titanium isopropoxide and the stabilizer acetylacetone.³⁹ The precursor solutions for the F-TiO_x films were prepared by mixing the appropriate concentrations of ammonium hexafluorotitanate ((NH₄)₂TiF₆, 99.99%, Aldrich) and boric acid (H₃BO₃). Both the solutions were separately stirred for at least 10 min at room temperature before mixing. The stirred solutions were mixed and placed in a pre-heated bath with temperature at 40 °C before immersing ITO substrates into the bath for F-TiO_x deposition. P3HT:PCBM blend was made in the ratio 1 : 0.8 (the concentration of P3HT was 15 mg ml⁻¹, whereas PCBM was 12 mg ml⁻¹) in 1 ml of dichlorobenzene (DCB). The mixed solution was stirred and heated at 60 °C overnight in a N₂ filled glove box prior to spin coating.

Device fabrication

Fluorinated TiO_x (F-TiO_x) was prepared *via* chemical bath deposition. The F-TiO_x film was deposited by immersing the ITO substrate into a chemical bath comprised of 0.1 M ammonium hexafluorotitanate ((NH₄)₂TiF₆) and 0.2 M boric

acid (H_3BO_3) at 40 °C for 90 min to obtain a film thickness of 80 nm. To control the fluorine concentration, the F-TiO_x samples were immersed in NaOH or ultrasonicated in de-ionised water for 30 min. Then, the films were rinsed with DI water after each treatment. Finally, the films were subjected to annealing at 180 °C for 1 h before proceeding to device fabrication. Inverted bulk heterojunction organic solar cells based on P3HT:PCBM were prepared on pre-patterned tin-doped indium oxide (ITO, Xinyan Technology Ltd.) coated glass substrates. The sheet resistance of the ITO (thickness: 90 ± 10 nm) was determined to be around 15–20 Ω □⁻¹. The substrates were pre-cleaned using a detergent solution, followed by successive ultrasonication in de-ionized water, isopropanol and acetone for 15 min each. Then, the substrates were dried in an oven at 60 °C for two hours. Then, 80 nm of fluorinated TiO_x (F-TiO_x) was deposited onto ITO *via* chemical bath deposition. For sol-gel TiO_x samples, the sol-gel precursor was spun on top of ITO substrates and hydrolyzed in a controlled environment (relative humidity 40%) for 2 h. All TiO_x films were annealed at 180 °C for 1 h in air before transferring to a N₂-filled glove box. For sol-gel TiO_x/F-TiO_x samples, the 40 nm of sol-gel precursor was first coated on ITO, hydrolyzed for 2 h and annealed at 180 °C for 1 h in air. After that, 40 nm of F-TiO_x was chemical bath deposited onto the sol-gel TiO_x in the abovementioned chemical bath and annealed at 180 °C for 1 h before transferring to a N₂-filled glove box. For F-TiO_x/sol-gel TiO_x samples, the 40 nm of F-TiO_x was chemical bath deposited onto the sol-gel TiO_x in the abovementioned chemical bath and annealed at 180 °C for 1 h. After that, 40 nm of sol-gel precursor was first coated on ITO, hydrolyzed for 2 h and annealed at 180 °C for 1 h before transferring to a N₂-filled glove box. P3HT:PCBM blend was spun onto the electron transport layer at 800 rpm for 30 s, and the resultant wet film was annealed on a hot plate at 140 °C for 1 min. The thickness of the photoactive layer was approximately 200 nm. Then, 70 nm of PEDOT:PSS blended with CFS-31 (PEDOT:PSS-CFS-31) with volume ratio of 5.5% was coated onto the active layer in air through a 0.45 μm cellulose filter and annealed at 140 °C for 1 min in the N₂ filled glove box. Then, Ag metal (100 nm) was thermally evaporated by a pre-designed shadow mask, resulting in an active device with an area of 9 mm². The vacuum condition during the evaporation was around 4 × 10⁻⁶ mbar. The completed device architecture is ITO/TiO_x/P3HT:PCBM/PEDOT:CFS-31/Ag. Cell degradation study was carried out by storing the device in a dark cabinet in open circuit conditions at 22 °C and relative humidity of 55%, in accordance with the ISOS-D-1 shelf scheme.³⁴

Material characterization

The current density–voltage (*j*–*V*) measurements were obtained under 1 sun illumination (ABET technologies Sun 2000 Solar Simulator) and a Keithley 2400 sourcemeter. The light-soaking treatment was done using the same lamp source, in which the devices were continuously illuminated and data were periodically acquired. The thicknesses of all layers were measured using Veeco DEKTAK 150 Stylus Profilometer. The electron microscopic images were obtained using JEOL FEG JSM 6700F

field emission SEM operating at 15 keV. All the fabrication steps, except coating of TiO_x and PEDOT:PSS, were performed inside a glove box of N₂ atmosphere (Charslton Technologies, ≤1 ppm moisture and O₂). X-ray photoelectron spectroscopy (XPS) measurements were performed using monochromatized Al-K_α at 1486.71 eV on a Kratos AXIS UltraDLD system. All the spectra were calibrated with respect to the C 1s spectrum (C–C bond) at 284.5 eV, and the peaks were fitted using Voigt (Gaussian and Lorentzian) function. Ultraviolet photoelectron spectroscopy (UPS) was performed with the same equipment, but with a He I (21.22 eV) radiation (VG Scientific ESCALab Mark 2) and applied bias of 5 V to separate the signals from samples and detector. The binding energies were set zero at the Fermi level. UV photocurrent response measurements were carried out using a Zahner impedance analyzer, equipped with a calibrated 365 nm UV light emitting diode (LED) source in ambient conditions. The light intensity of the LED, which was regulated by a photosensor in a control loop, was set at 50 W m⁻². The UV light source was time-programmed accordingly for periodic power on and off. TiO_x/Ag with two parallel Ag contacts were used as the measurement devices. They were biased at 0.01 V in all measurements.

Acknowledgements

SERIS is sponsored by the National University of Singapore (NUS) and Singapore's National Research Foundation (NRF) through the Singapore Economic Development Board (EDB). Fang Jeng Lim would also like to express his sincere gratitude to Singapore National Research Foundation (Energy Innovation Programme Office) for providing a PhD scholarship. We gratefully acknowledge Dupont™ through MegaChem Limited, Singapore for supplying Capstone® FS-31.

References

- 1 A. K. K. Kyaw, D. H. Wang, V. Gupta, J. Zhang, S. Chand, G. C. Bazan and A. J. Heeger, *Adv. Mater.*, 2013, **25**(17), 2397–2402.
- 2 M. Song, J. W. Kang, D. H. Kim, J. D. Kwon, S. G. Park, S. Nam, S. Jo, S. Y. Ryu and C. S. Kim, *Appl. Phys. Lett.*, 2013, **102**(14), 143303.
- 3 F. J. Lim, A. Krishnamoorthy, J. Luther and G. W. Ho, *J. Mater. Chem.*, 2012, **22**(48), 25057–25064.
- 4 S. Woo, W. H. Kim, H. Kim, Y. Yi, H. K. Lyu and Y. Kim, *Adv. Energy Mater.*, 2014, **4**, 1301692.
- 5 J. Kim, G. Kim, Y. Choi, J. Lee, S. H. Park and K. Lee, *J. Appl. Phys.*, 2012, **111**(11), 114511.
- 6 T. Kuwabara, C. Iwata, T. Yamaguchi and K. Takahashi, *ACS Appl. Mater. Interfaces*, 2010, **2**(8), 2254–2260.
- 7 O. Pachoumi, C. Li, Y. Vaynzof, K. K. Banger and H. Sirringhaus, *Adv. Energy Mater.*, 2013, **3**(11), 1428–1436.
- 8 W. Wei, C. Zhang, D. Chen, Z. Wang, C. Zhu, J. Zhang, X. Lu and Y. Hao, *ACS Appl. Mater. Interfaces*, 2013, **5**(24), 13318–13324.
- 9 F. C. Krebs, T. Tromholt and M. Jørgensen, *Nanoscale*, 2010, **2**(6), 873–886.

- 10 S. Trost, K. Zilberberg, A. Behrendt, A. Polywka, P. Görrn, P. Reckers, J. Maibach, T. Mayer and T. Riedl, *Adv. Energy Mater.*, 2013, **3**(11), 1437–1444.
- 11 M. R. Lilliedal, A. J. Medford, M. V. Madsen, K. Norrman and F. C. Krebs, *Sol. Energy Mater. Sol. Cells*, 2010, **94**(12), 2018–2031.
- 12 Z. Lin and J. Zhang, *ACS Appl. Mater. Interfaces*, 2013, **5**(3), 713–718.
- 13 H. Schmidt, K. Zilberberg, S. Schmale, H. Flügge, T. Riedl and W. Kowalsky, *Appl. Phys. Lett.*, 2010, **96**(24), 243305.
- 14 J. C. Wang, C. Y. Lu, J. L. Hsu, M. K. Lee, Y. R. Hong, T. P. Perng, S. F. Horng and H. F. Meng, *J. Mater. Chem.*, 2011, **21**(15), 5723–5728.
- 15 M. K. Lee, C. H. Fan, H. C. Wang and C. Y. Chang, *J. Electrochem. Soc.*, 2011, **158**(8), D511–D514.
- 16 C. Lei, H. Zhou, Z. Feng, Y. Zhu and R. Du, *J. Alloys Compd.*, 2012, **513**(5), 552–558.
- 17 Y. Wang, H. Zhang, P. Liu, T. Sun, Y. Li, H. Yang, X. Yao and H. Zhao, *J. Mater. Chem. A*, 2013, **1**(41), 12948–12953.
- 18 M. Samadpour and J. Bisquert, *J. Phys. Chem. C*, 2011, **115**(29), 14400–14407.
- 19 S. Pawar, B. Pawar, J. Kim, O. S. Joo and C. Lokhande, *Curr. Appl. Phys.*, 2011, **11**(2), 117–161.
- 20 H. Khallaf, C. T. Chen, L. B. Chang, O. Lupan, A. Dutta, H. Heinrich, F. Haque, E. D. Barco and L. Chow, *Appl. Surf. Sci.*, 2012, **258**(16), 6069–6074.
- 21 C. Lokhande, *Mater. Chem. Phys.*, 1991, **27**(1), 1–43.
- 22 T. Kuwabara, H. Sugiyama, M. Kuzuba, T. Yamaguchi and K. Takahashi, *Org. Electron.*, 2010, **11**(6), 1136–1140.
- 23 Y. Masuda and K. Kato, *Thin Solid Films*, 2008, **516**(9), 2547–2552.
- 24 S. Supothina and M. De Guire, *Thin Solid Films*, 2000, **371**(1), 1–9.
- 25 A. More, T. Gujar, J. Gunjekar, C. Lokhande and O. S. Joo, *Appl. Surf. Sci.*, 2008, **255**(5), 2682–2687.
- 26 H. C. Cheng, C. F. Chen and C. C. Lee, *Thin Solid Films*, 2006, **498**(1–2), 142–145.
- 27 H. Han, P. Sudhagar, T. Song, Y. Jeon, I. Mora-Sero, F. Fabregat-Santiago, J. Bisquert, Y. S. Kang and U. Paik, *Phys. Chem. Chem. Phys.*, 2013, **49**(27), 2810–2812.
- 28 S. Deki, Y. Aoi, Y. Asaoka, A. Kajinami and M. Mizuhata, *J. Mater. Chem.*, 1997, 733–736.
- 29 L. M. Chen, Z. Xu, Z. Hong and Y. Yang, *J. Mater. Chem.*, 2010, **20**, 2575–2598.
- 30 S. Liu and M. Jaroniec, *J. Am. Chem. Soc.*, 2010, **132**(34), 11914–11916.
- 31 Q. Wang, W. Ma and J. Zhao, *Langmuir*, 2008, **24**(14), 7338–7345.
- 32 K. Lv, B. Cheng, J. Yu and G. Liu, *Phys. Chem. Chem. Phys.*, 2012, **14**(16), 5349–5362.
- 33 B. Ecker, H. J. Egelhaaf, R. Steim, J. Parisi and E. V. Hauff, *J. Phys. Chem. C*, 2012, **116**(31), 16333–16337.
- 34 M. Reese, S. Gevorgyan, M. Jørgensen, E. Bundgaard, S. Kurtz, D. Ginley, D. Olson, M. Lloyd, P. Morvillo and E. Katz, *Sol. Energy Mater. Sol. Cells*, 2011, **95**(5), 1253–1267.
- 35 M. T. Lloyd, D. C. Olson, P. Lu, E. Fang, D. L. Moore, M. S. White, M. O. Reese, D. S. Ginley and J. W. P. Hsu, *Phys. Chem. Chem. Phys.*, 2009, **19**(41), 7638–7642.
- 36 J. Kim, C. Kim, Y. Kim and Y. Loo, *Appl. Phys. Lett.*, 2009, **95**, 183301.
- 37 K. Pomoni, A. Vomvas and C. Trapalis, *Thin Solid Films*, 2005, **479**(1–2), 160–165.
- 38 W. Q. Fang, X. L. Wang, H. Zhang, Y. Jia, Z. Huo, Z. Li, H. Zhao, H. G. Yang and X. Yao, *J. Mater. Chem. A*, 2014, **2**(10), 3513–3520.
- 39 T. Kuwabara, T. Nakayama, K. Uozumi, T. Yamaguchi and K. Takahashi, *Sol. Energy Mater. Sol. Cells*, 2008, **92**(11), 1476–1482.